Chapter 4

Phase Segregation Assisted Morphology Sculpting 1. Growth of Graphite via Vapor-Solid Reaction

4.1 Introduction

Varying morphology, including shape and dimensionality, and tuning sizes of nanostructures may provide means to tailor physical and chemical properties of functional materials. Many studies have demonstrated how to achieve the control through various synthetic strategies.[1-7] These include reactions performed under mild conditions such as chemical precipitation, sol, micelle, and sol-gel processes. In addition, there are processes demanding vigorous conditions, for example, hydrothermal synthesis, pyrolysis, and vapor deposition.[8] Carbon, a technologically important material, can been synthesized via several unrelated methods into porous, fibrous and lamellar forms.[9-13] Herein, we report that highly graphitized carbon materials can be synthesized via a simple vapor-solid reaction growth (VSRG)[14-16] by reacting CaC_2 with organoperchloro compounds C_xCl_y at relatively low temperatures 973 – 1223 K. More strikingly, we observed that morphology of the as-formed carbon nanostructures can be directly manipulated simply by varying the reaction temperatures. This appears to be an action of phase segregation of the solid products carbon and $CaCl_2$ formed in the reaction. The observation is a parallel to minerals formed in the earth's crust. In nature, spherical, porous, fibrous, dendridic and other shaped crystals appear in multiphase rocks solidified under various conditions.[17,18] Moreover, the observed morphology alteration of the carbon material is analogous to phase segregation in diblock and triblock copolymer systems.[19,20] In these systems, due to chemical incompatibility, each one of different component blocks self-assembles into various ordered nanophases. Cooperatively, they generate spherical, cylindrical and lamellar structures.[21,22] Our

discoveries are reported below.

4.2 Experimental Section

4.2.1 Synthesis

C_xCl_y were purchased either from Aldrich (CCl_4, 99.5%; C_2Cl_4, 99%; C_5Cl_6, 98 %) or from ACROS (C_4Cl_6, 98 %) [Caution! LD_{50} (g kg^{-1}) oral for CCl_4: 3.6 (mouse), C_2Cl_4: 6.4 (rat), C_4Cl_6: 0.09 (mouse) and C_5Cl_6: 0.5 (rat)]. CaC_2 (80 %) was supplied by Aldrich (Caution! CaC_2 drastically reacts with water to produce flammable acetylene gas). Different experimental parameters of the reactions between C_xCl_y and CaC_2 are listed in Table 4.1. A reaction employed C_4Cl_6 to react with CaC_2 is described below as an example.

In a tubular reactor at 1223 K under 1 atm, powders of CaC_2 (0.5 g) in an aluminum oxide boat were allowed to react with C_4Cl_6 evaporated at 333 K under bubbling Ar (30 sccm) for 18 h. The as-prepared black products were further washed twice in refluxing distilled water (300 mL) overnight to remove $CaCl_2$. A purified black product (0.28 g) was obtained. The results will be discussed in the text below and shown in the supporting information.

4.2.2 Characterization

Morphology and structure of the products were evaluated using a scanning electron microscope (SEM, JEOL JSM-6330F, operated at 15 kV). Energy dispersive X-ray spectroscopy (EDS) was used to confirm the element composition of the samples. a transmission electron microscope (TEM, JEOL JEM-4000EX, operated at 400 kV), an X-ray diffractometer (XRD, Bruker D8 Advance, Kα radiation at 40 kV and 40 mA) and a Raman spectrometer (Jabin-Yvon T-64000 with the incident wavelength at 514.5 nm).

4.3. Results

Solids of CaC_2 were reacted with vapors of C_xCl_y (CCl_4, C_2Cl_4, C_5Cl_6, C_4Cl_6) at elevated temperatures 973 – 1223 K to offer black raw products. Table 4.1 summarizes the reaction parameters and the results of characterization, which will be discussed below.

Table 4.1 Summary of reaction conditions and product morphology.

Precursor	Vaporization condition[a]	Reaction temperature (K)	Graphite product morphologies[b]	La (nm)	Lc (nm)
CCl_4	5 sccm at 255 K, 1 atm	1023	**Porous**. Pore size: 400 - 650 nm; wall thickness: 100 - 180 nm	2.65	1.01
		1123	**Fibrous**. Diameter: 80 - 110 nm; length: tens of micrometers	3.47	7.15
		1223	**Planar**. Thickness: 70 - 150 nm; plate diameter: 1 - 4 μm	4.57	8.42
C_2Cl_4	5 sccm at 298 K, 1 atm	973	**Porous**. Pore size: 250 nm - 1 μm; wall thickness: 20 - 70 nm	2.43	1.03
		1073	**Fibrous**. Diameter: 25 - 45 nm; length: tens of micrometers	2.81	2.41
		1123	**Planar**. Thickness: 15 - 75 nm; plate diameter: 500 nm - 3 μm	2.87	5.31
C_4Cl_6	30 sccm at 333 K, 1 atm	1023	**Porous**. Pore size: 50 nm - 400 nm; wall thickness: 15 – 45 nm	2.94	1.45
		1123	**Fibrous**. Diameter: 60 - 120 nm; length: 1 - 3 μm	5.57	9.61
		1223	**Planar**. Thickness: 15 - 60 nm; plate diameter: 400 nm - 1 μm	9.66	9.81
C_5Cl_6	5 sccm at 281 K, 1 atm	1023	**Porous**. Pore size: 150 nm - 1.5 μm; wall thickness: 100 - 400 nm	2.81	1.35
		1123	**Fibrous**. Diameter: 35 - 60 nm; length: 1.5 - 2 μm	4.18	7.74
		1223	**Planar**. Thickness:100 - 200 nm; plate diameter: several μm	7.80	9.49

a. Precursors bubbled under Ar gas.

b. Carbon products morphologies observed from SEM and TEM images

4.3.1 Morphology Studies by SEM

Images of some typical raw products formed from the reactions between CaC_2 and C_xCl_y are shown in Figure 4.1. Using CCl_4, ball-shaped particles are formed at 1023 K as the raw product, as shown in Figure 4.1A. Several ripped particles displayed in the image also suggest that the balls may have a core-shell structure. Energy dispersive X-ray spectrum (EDS) (Figure 4.1B) of the product shows the presence of C, Ca and Cl. Common chemical knowledge would suggest that the product is a composite of C and $CaCl_2$. The presence of $CaCl_2$ is confirmed by an XRD study. In addition to reflections from graphite, which will be discussed further below, reflections from $CaCl_2(H_2O)_x$, $CaCl_2$ hydrated in moist air, were also observed. Figure 4.1C shows the sample obtained from the reaction between CaC_2 and CCl_4 at 1123 K. The image demonstrates light and dark stripes on the surface. EDS (Figure 4.1D) also shows that the sample contains C, Ca and Cl. At 1223 K, the observed product from the reaction involving CaC_2 and C_5Cl_6, as shown in Figure 4.1E, is aggregates of thin plates. Signals from C, Ca and Cl atoms are detected in Figure 4.1F.

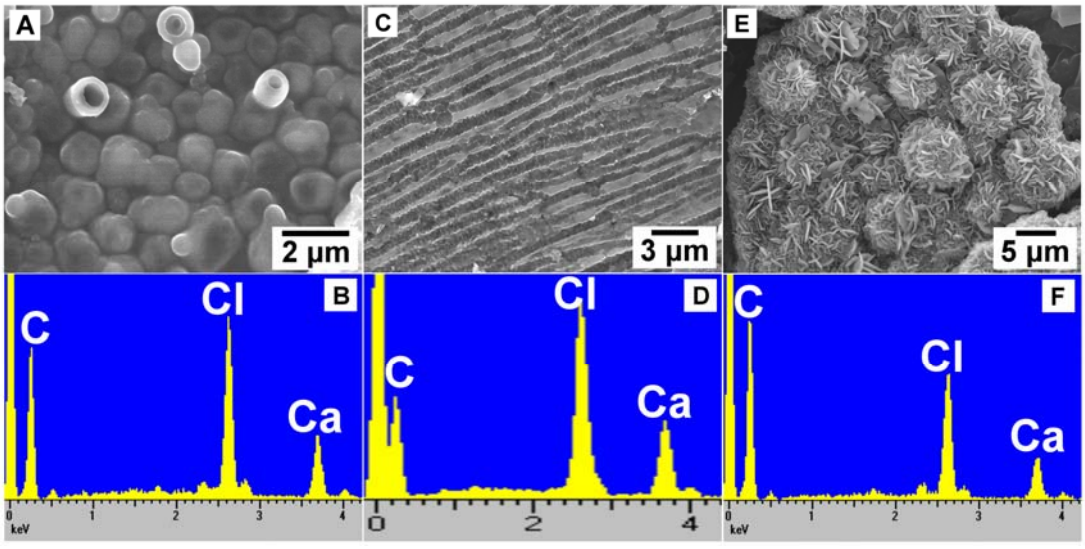

Figure 4.1 SEM and EDS graphite/$CaCl_2$ nanostructures synthesized from CaC_2 and C_xCl_y. (A) SEM and (B) EDS of the as-prepared product grown at 1023 K from CCl_4; (C) SEM and (D) EDS of the as-prepared product grown at 1123 K from CCl_4; (E) SEM and (F) EDS of the as-prepared product grown at 1223 K from C_5Cl_6.

Raw products were washed by distilled water for a long period of time to remove $CaCl_2$. Images of purified examples, prepared from the reactions between CaC_2 and C_4Cl_6, are shown in Figure 4.2. The SEM image in Figure 4.2A suggests that the sample synthesized at 1023 K contains innumerable pores. A TEM study revealed that the pore size was 50 – 400 nm while the thickness was 15 – 45 nm. Increasing the reaction temperature to 1123 K, a one-dimensional fibrous material (diameter 60 – 120 nm and length 1 – 3 μm by TEM), shown in Figure 4.2B, is isolated. The product formed at 1223 K shows mainly thin planar structure (thickness 15 – 60 nm and width 0.4 – 1 μm by TEM) in Figure 4.2C. EDS spectra confirmed that the solid products are composed mainly of carbon. No other signals were observed. Reactions employing various organoperchloro compounds displayed very similar correlation between reaction temperature and product morphology shown in Figure 4.3 and Figure 4.4. The structure changed from porous to fibrous, then to lamellar as the reaction temperature was raised. Also, for all reactions, morphology of the raw products (Figure 4.1) compared well with that of the samples free of $CaCl_2$ (Figure 4.2-4.4). This suggests that the products were shaped by segregated salt and carbon phases cooperatively.

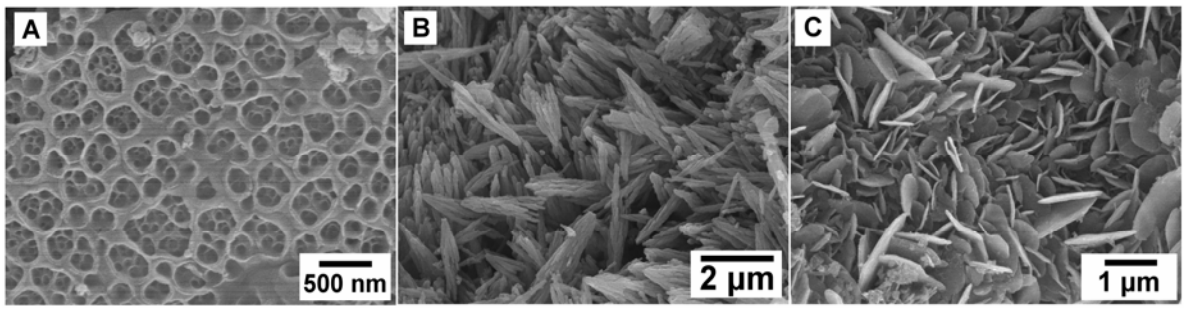

Figure 4.2 SEM images of graphite products prepared from CaC_2 and C_4Cl_6 products after the removed of $CaCl_2$. (A) porous carbon, prepared at 1023 K; (B) fibrous carbon, prepared at 1123 K; (C) planar carbon, prepared at 1223 K.

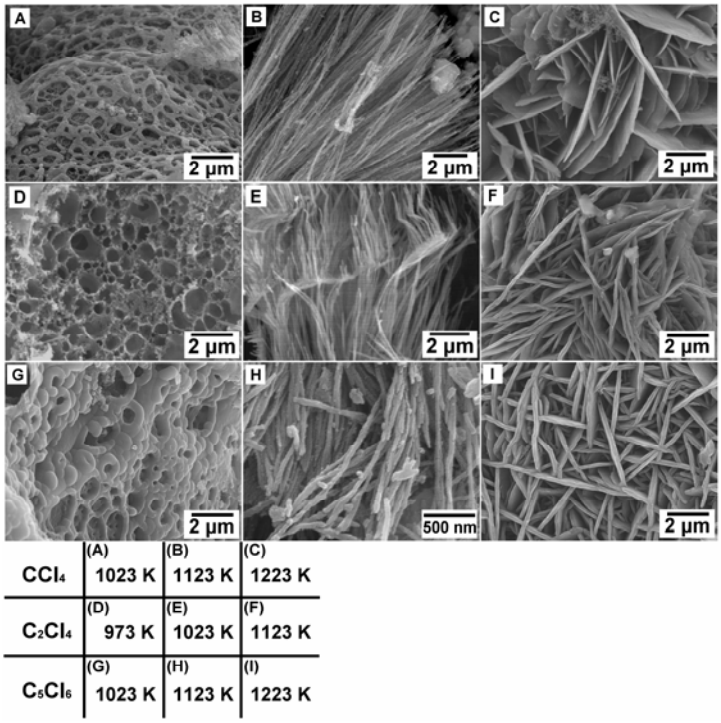

Figure 4.3 SEM images of graphite products prepared from CaC_2 and C_xCl_y at different temperatures.

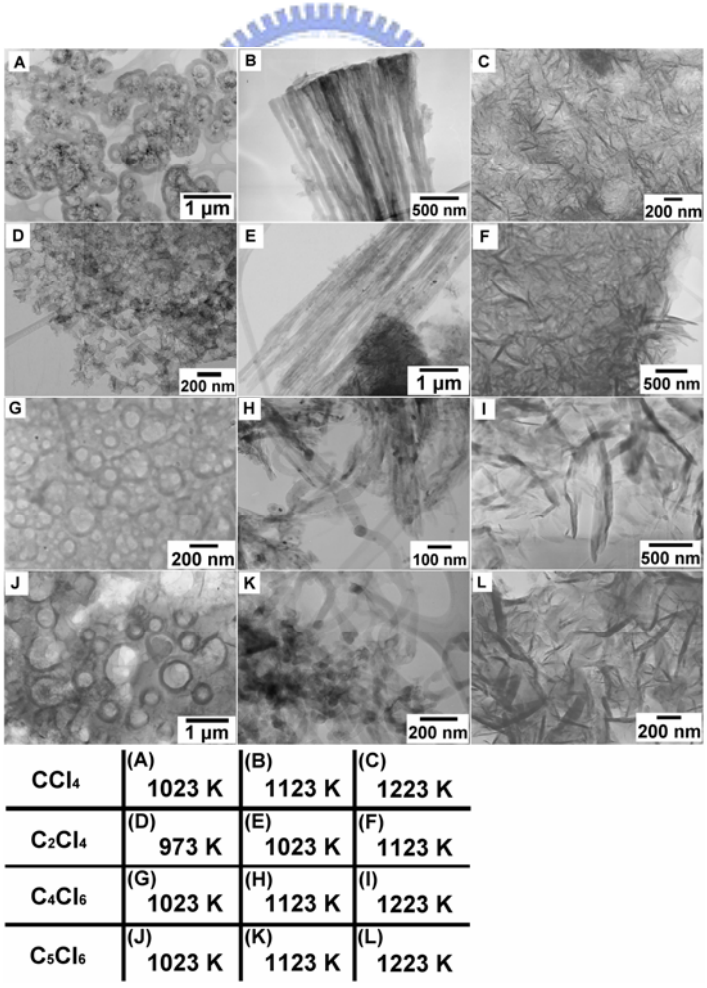

Figure 4.4 TEM images of graphite products prepared from CaC_2 and C_xCl_y at different temperature.

4.3.2 Structural Characterization by XRD, Raman and HRTEM

The co-existence of $CaCl_2$ and grapgite is observed by XRD shown in Fighre 4.5. The $CaCl_2(H_2O)_x$ is presented due to the $CaCl_2$ hydrated in moist air. XRD was employed to structurally characterize the purified products. The data of samples synthesized from the reactions between C_4Cl_6 and CaC_2, are shown in Figure 4.6A as an example. The patterns show major reflections with increasing intensity at 2θ 25.5° (d = 0.350 nm), 26.0° (d = 0.342 nm) and 26.2° (d = 0.340 nm) for the samples grown at 1023 K, 1123 K and 1223 K, respectively. These are slightly larger than the (002) reflection of graphite (JCPDS 23-0064), observed at 2θ 26.5° (d = 0.336 nm).

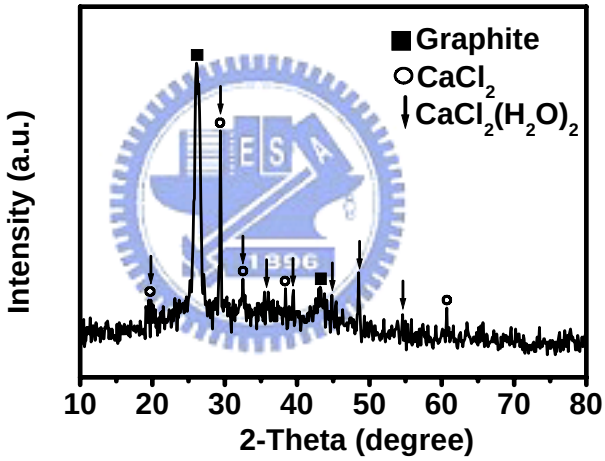

Figure 4.5 XRD of graphite/$CaCl_2(H_2O)_x$ product grown from C_4Cl_6 at 1223 K.

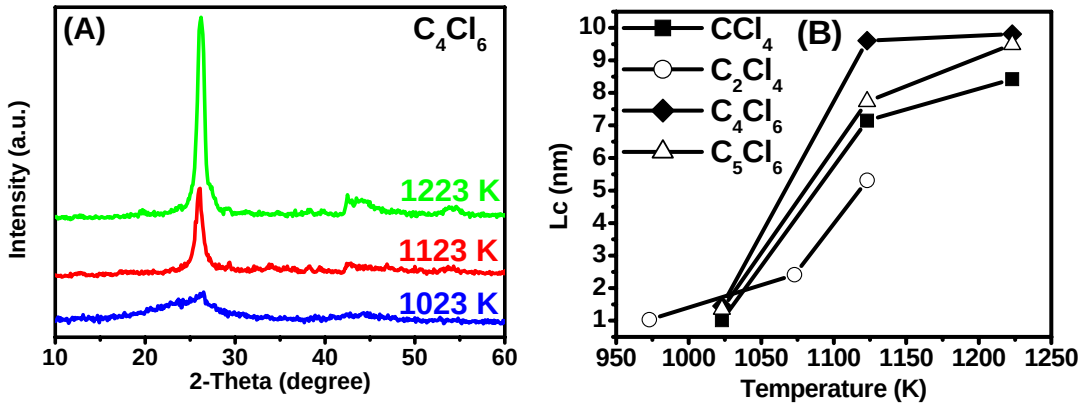

Figure 4.6 (A) XRD of graphite products grown at 1023 K ─ 1223 K from C_4Cl_6; (B) Crystal size Lc of the graphite prepared from CaC_2 and C_xCl_y at different temperatures.

The value Lc, stacking height of layer planes, can be calculated using Scherrer equation. Lc is an estimate of repeating orderness of the graphite layers, which is the thickness of graphite domains.[23] In Figure 4.6B, the Lc data are plotted against the reaction temperature. In general, Lc, an index of crystallinity, increases with the increasing temperature. Among the organoperchloro compounds employed, the samples prepared from C_4Cl_6 offer the optimum result. The highest Lc, 9.81 nm, is observed for a sample grown at 1223 K. This is comparable to Lc of a synthesized graphitic carbon material, which is heat treated above 2773 K, 6 - 8 nm.[24,25]. Also, the crystallite size of natural graphite is around 22 nm.[26] The other XRD patterns of C_xCl_y react with CaC_2 are displayed in Figure 4.7.

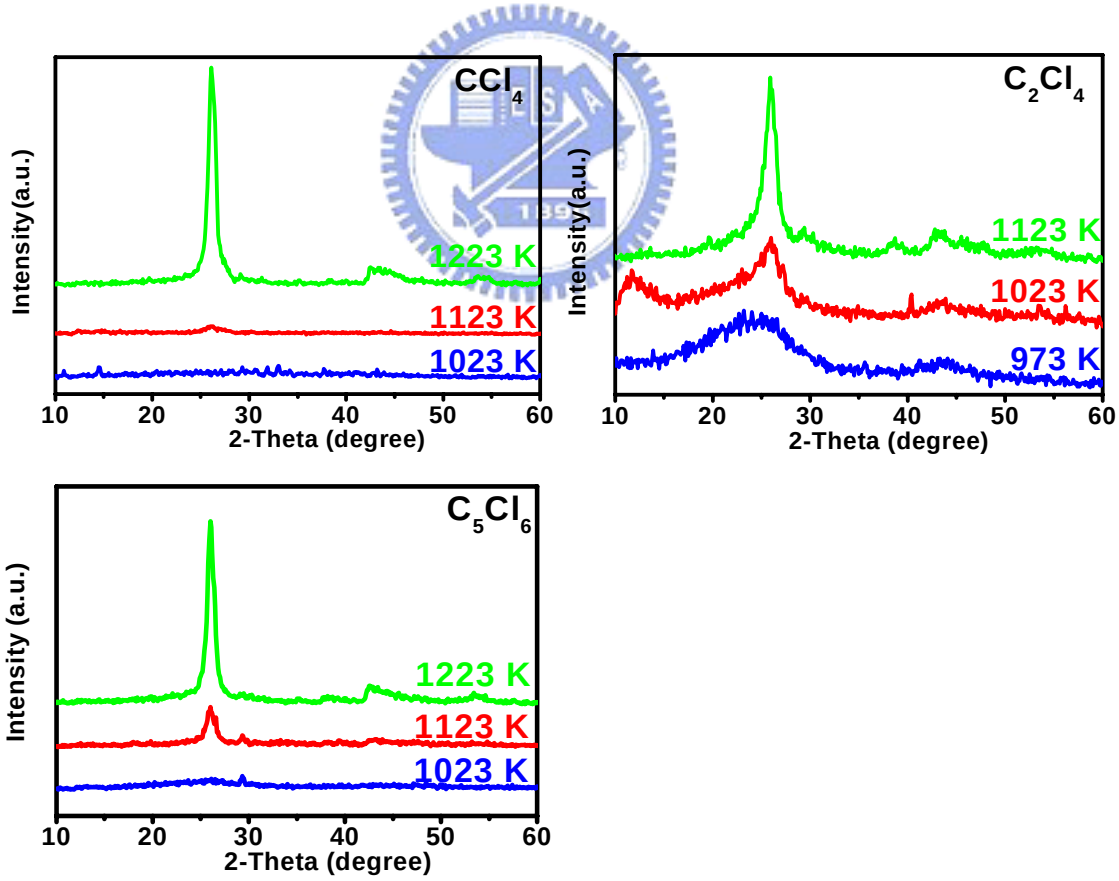

Figure 4.7. XRD of graphite products grown at 973 K ─ 1223 K from CaC_2 and C_xCl_y.

Raman spectroscopy is another method frequently used to estimate the crystallinity of carbon materials. A sharp vibration mode at 1580 cm^{-1}, called the first-order G band, is due to sp^2-bonded carbon domains in crystalline graphite. The peak at around 1360 cm^{-1} is regarded as disordered structure and is labeled as the D band. The value La, which shows approximate orderness in graphite hexagonal planes, is directly proportional to the inverse of intensity ratio between D and G bands, I_D/I_G.[27] Figure 4.8A displays the Raman spectra of the products grown from C_4Cl_6 at 1023 – 1223 K. All spectra display the D and the G bands at 1580 cm^{-1} and 1360 cm^{-1}, respectively. The D band signal intensity decreases with the increasing reaction temperature, indicating that I_D/I_G increases very significantly. Consequently, as shown in Figure 4.8B, the La value increases as the reaction temperature raised. This suggests that the graphite domain size expands and forms highly oriented structure at high reaction temperatures. Among, the organoperchloro compounds employed, C_4Cl_6 also shows the optimum La result. The La value is 9.66 nm. This is also comparable to the La values of other graphites synthesized at high temperatures. They are smaller than 10 nm.[28-30] The La value for commercial graphite, which has been processed at high temperature for a long period of time, is 31.7 nm.[31] The detailed value of Lc and La are listed in Table 4.1. The Raman spectra of other organoperchloro show in Figure 4.9.

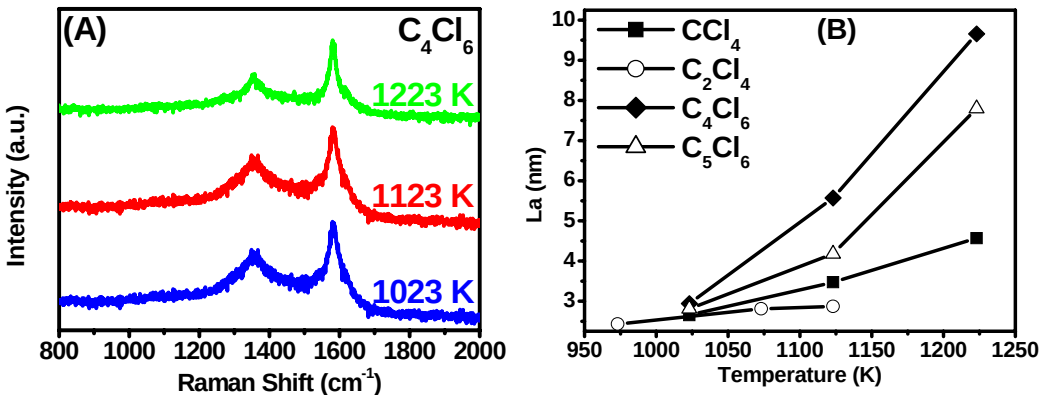

Figure 4.8 (A) Raman spectra of graphite products grown at 1023 K ─ 1223 K from C_4Cl_6. (B) Crystal size La of the graphite prepared from CaC_2 and C_xCl_y at different temperatures.

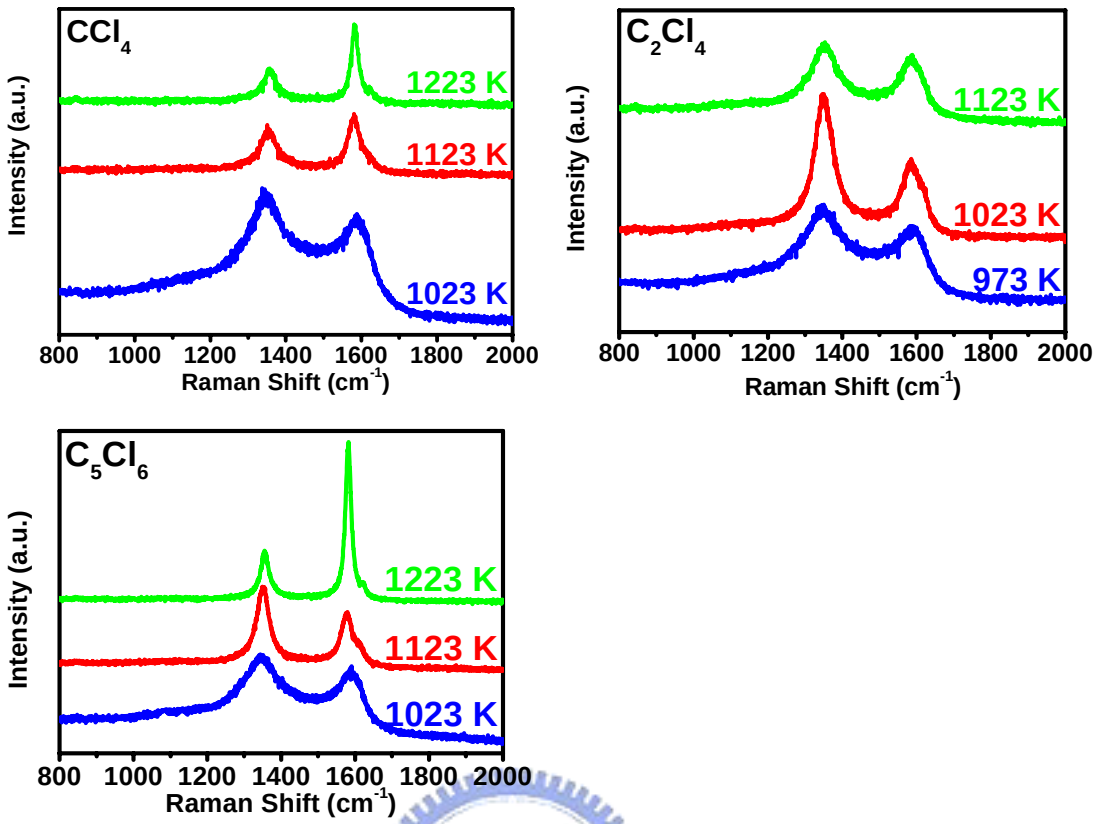

Figure 4.9 Raman spectra of graphite products grown at 973 K ─ 1223 K from CaC_2 and C_xCl_y.

Figure 4.10 shows high resolution TEM (HRTEM) images of the materials prepared from CaC_2 and C_4Cl_6. The interlayer spacing, which corresponds to the (002) distance of graphite carbon, decreases from 0.341 nm to 0.336 nm as the reaction temperature is increased from 1023 to 1223 K. The data agree with the d spacing values estimated from the selected area electron diffraction (SAED) patterns shown in the insets of Figure 4.10. The SAED pattern in Figure 4.10A shows a double ring-like pattern, indicating a less ordered microcrystalline structure, while those in Figures 4.10B and 4.10C display dot patterns, suggesting more extended crystal ordering. The ordering of the graphite layer appears to be extensive. For example, an HRTEM image of a fibrous sample prepared from C_4Cl_6 at 1023 K showed that the material contained up to 100 layers of graphite sheets with the planes aligned to the fiber axis shown in Figure 4.11.

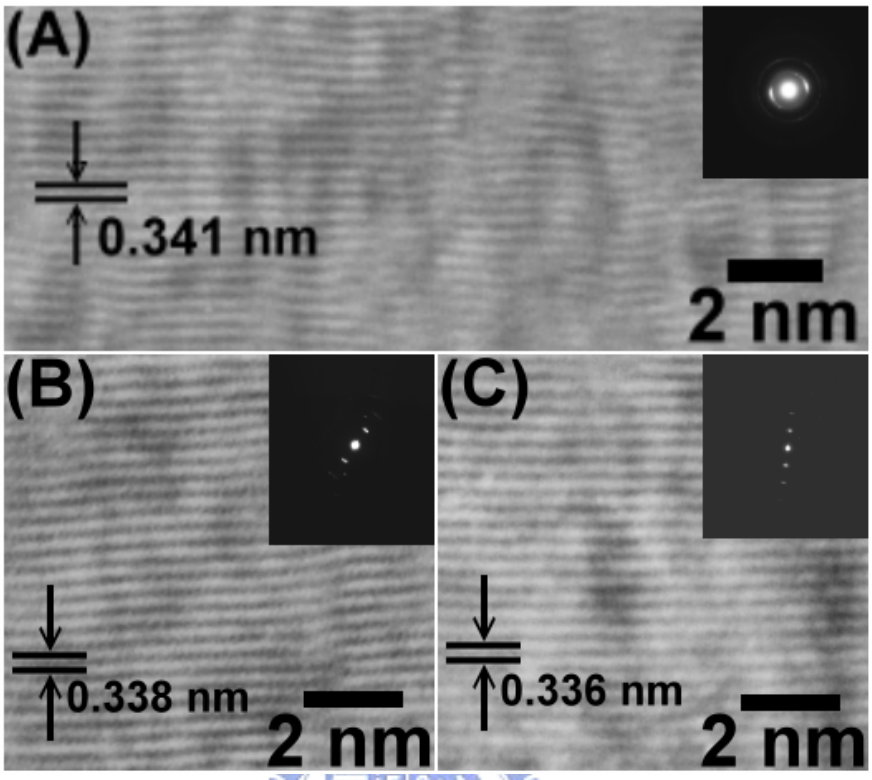

Figure 4.10 HRTEM and SAED (inset) images of graphite grown from CaC_2 and C_4Cl_6 at (A) 1023 K; (B) 1123 K; (C) 1223 K.

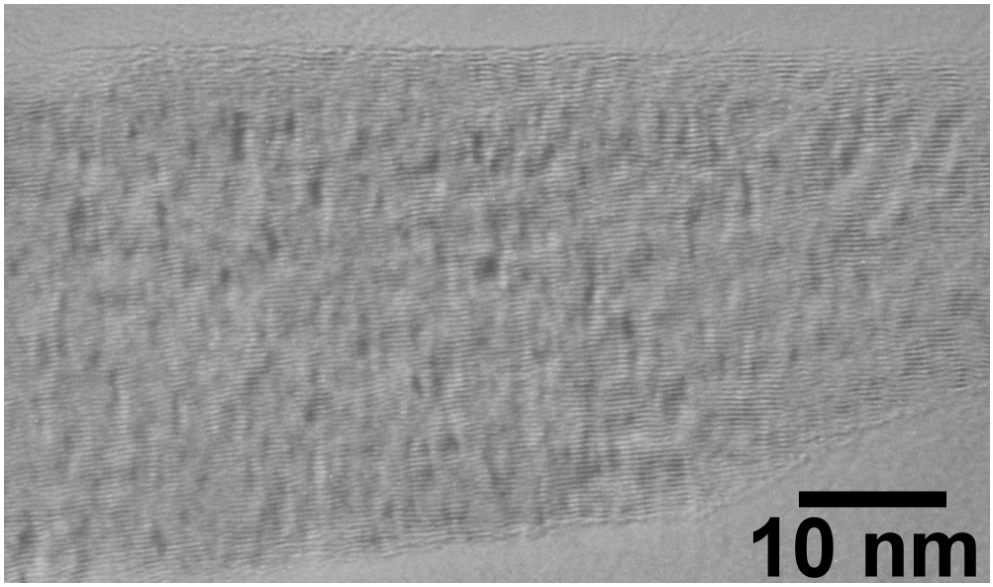

Figure 4.11 HRTEM of a sample prepared from CaC_2 and C_4Cl_6 at 1023 K, showing nearly 100 graphite layer.

4.4 Discussion

4.4.1 Morphology Alteration by Phase Segregation

An illustrated reaction pathway for fabrication porous, fibrous and lamellar carbon materials from CaC_2 and C_xCl_y is shown in Scheme 4.1. At different temperatures, the products $CaCl_2$ and C, with large difference in surface energies, undergo phase segregation and templating each other cooperatively into the observed morphology. In polymer science, many researchers have examined morphology alteration caused by phase segregation in block copolymer systems.[32,33] They have discovered that the following parameters affect the structure and morphology of block copolymers greatly: χN (χ is the Flory parameter characterizing A-B interactions; N is the polymer index) which is dependant on temperature, and *f* (*f* is the fraction of monomers A in a chain). In many ways, the phenomenon observed in copolymer systems parallels to what observed in this study. In our system, the overall product morphology is more strongly affected by reaction temperature but less significantly by reactants nature.

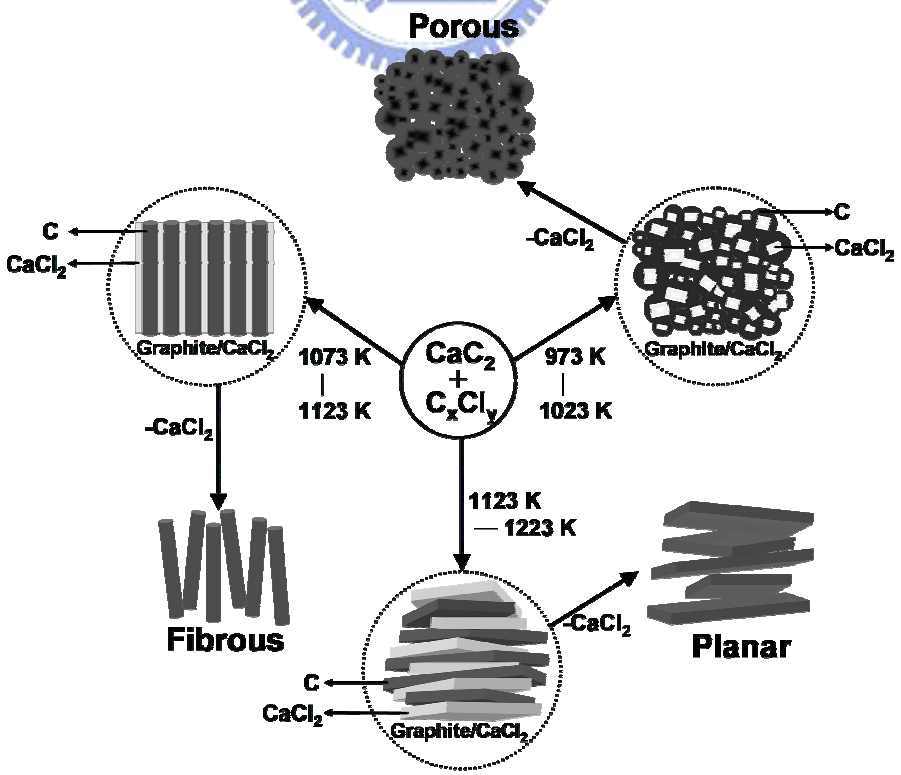

Scheme 4.1 Summary of textured graphite formation from the reaction between CaC_2 and C_xCl_y.

In general, porous carbon is produced at low reaction temperatures 973 - 1023 K. In the medium temperatures 1073 - 1123 K, fibrous carbon is the major product. Finally, planar carbon is synthesized at high reaction temperatures 1123 - 1223 K. The graphite products formed from C_4Cl_6 are special. They are generally more ordered than the other ones form at the same temperatures. This will be discussed further in the next section.

4.4.2 Low Temperature Graphitization

In common practice, it frequently requires high temperature (> 2273 K) graphitization processes to align atoms in disordered carbon materials.[34] It is interesting to note that in this study, comparatively ordered graphite materials can be grown at temperatures as low as 1023 K. This is probably due to the exothermic nature of these reactions, which provide energetically favored local reaction sites. For example, the estimated standard enthalpy of reaction ΔH_r^o is - 689 kJ/mole of CaC_2 consumed in the reaction between CaC_2 and CCl_4.[35] In another case employing C_4Cl_6 as the reactant, which generates more ordered products with higher La and Lc values at comparable temperatures, ΔH_r^o is more exothermic – 728 kJ/mol of CaC_2 used.[35] At the first glance, the higher ΔH_r^o appear to be the cause for the formation of more ordered products in the case involving C_4Cl_6. On the other hand, for the reaction employing C_2Cl_4, a calculation shows an indistinguishable ΔH_r^o of - 730 kJ/mol of CaC_2 used.[35] In the study, we discovered that the carbon products prepared from C_2Cl_4 did not show the same degree of orderness as the one formed from C_4Cl_6. Thus, the difference in thermodynamics among reactions alone cannot explain why using C_4Cl_6 can produce products as ordered as graphites heated at 2473 K.[28] A better rationalization is that the reaction between CaC_2 and C_4Cl_6 may proceed via an energetically favored inverse Diels-Alder reaction mechanism.[36] In a CaC_2 lattice, electron-rich π bonds of C_2^{2-} units may act as dienophiles while C_4Cl_6 molecules, due to the presence of electron withdrawing Cl atoms, can be viewed as electron-poor dienes. In an inverse Diels-Alder reaction, the HOMO-dienophile to LUMO-diene interaction would provide a low energy barrier pathway

to overcome the reaction barrier and to generate six-membered C_6 rings, the basic components of graphite.[37,38] The kinetic reason could explain why more graphitized carbon materials are grown in the reaction using C_4Cl_6 than in the ones using other C_xCl_y molecules.

4.4.3 Effect of CaX_2 (X= F, Cl) salts

It is interesting to note that in an analogous reaction between CaC_2 and C_6F_6 at 973 K, growth of phase-segregated CaF_2/*a*-C core-shell nanowires were observed.[16] The morphology and crystallinity of the product showed significant difference from the ones produced in this study. There are several possible reasons to explain the differences. The first one is that the melting point (m.p.) of $CaCl_2$, 1045 K, is significantly lower than that of CaF_2, 1676 K. Based on the information, we may conclude that $CaCl_2$ may exist in a flexible molten state in the phase segregated products during the reactions. The self-templating process would sculpt the graphite into a wide range of morphology. An analogous observation has been discovered in reactions between $SiCl_4$ and silicides of group II metals Mg_2Si and $CaSi_2$.[39] The other possible reason may originate from the difference between C-F and C-Cl bond strengths, 443 kJ/mol and 339 kJ/mol, respectively.[40] The strong C-F bond in the precursor molecule may lead to incomplete C-F bond breaking during the reactions. The residual C-F bonds may disarray the carbon into graphite layers. They may also form good interfacial bindings between carbon and CaF_2 phases. In contrast, the C-Cl bonds should break more readily. The interfacial binding between carbon layers and $CaCl_2$ is weak due to large difference in surface energies. This would assist the separation of molten $CaCl_2$ and solid carbon into different product morphology. The observation parallels the phase segregation phenomenon in diblock and triblock copolymer systems.[19,20] Also, we speculate that morphology of many rocks and minerals may arrive via an analogous pathway.[17,18]

4.5 Conclusions

In summary, we have demonstrated the first time that alternation of graphite nanostructures with three different morphologies can be achieved easily via a simple VSRG reaction between CaC_2 and organoperchloro compounds at favorable reaction temperatures. The reaction proceeds without assistance from added template and catalyst materials, employment of special source of energies, and utilization of special pressure reactors. The graphite is highly influenced by the other phase-segregated product $CaCl_2$, which acts as a self-template to sculpt the product morphology. Using C_4Cl_6, highly ordered graphitic products are grown. We attribute this achievement to the assistance of an inverse Diels-alder reaction pathway. We expect these uniquely shaped graphite materials will find many special applications in the future.

References

(1) Milliron, D. J.; Hughes, S. M.; Cui, Y.; Manna, L.; Li, J.; Wang, L.-W.; Alivisatos, A. P. *Nature* **2004**, *430*, 190-195.

(2) Peng, X.; Manna, L.; Yang, W.; Wickham, J.; Scher, E.; Kadavanich, A.; Alivisatos, A. P. *Nature* **2000**, *404*, 59-61.

(3) Pileni, M. *Nat. Mater.* **2003**, *2*, 145-150.

(4) Kim, F.; Connor, S.; Sond, H.; Kuykendall, T.; Yang, P. *Angew. Chem.* **2004**, *43*, 3673-3677.

(5) Chen, J.; Herricks, T.; Xia, Y. *Angew. Chem.* **2005**, *44*, 2589-2592.

(6) Yu, T.; Joo, J.; Park, Y. I.; Hyeon, T. *Angew. Chem.* **2005**, *44*, 7411-7414.

(7) Tapan, T. K.; Murphy, C. J. *J. Am. Chem. Soc.* **2004**, *126*, 8648-8649.

(8) Burda, C.; Chen, X.; Narayanan, R.; El-Sayed, M. A. *Chem. Rev.* **2005**, *105*, 1025-1102.

(9) Liang, C.; Hong, K.; Guiochon, G. A.; Mays, J. W.; Dai, S. *Angew. Chem.* **2004**, *43*, 5785-5789.

(10) Yu, J.-S.; Kang, S.; Yoon, S. B.; Chai, G. *J. Am. Chem. Soc.* **2002**, *124*, 9382-9383.

(11) Ryoo, R.; Joo, S. H.; Kruk, M.; Jaroniec, M. *Adv. Mater.* **2001**, *13*, 677-681.

(12) Lim, S.; Yoon, S.-H.; Shimizu, Y.; Jung, H.; Mochida, I. *Langmuir* **2004**, *20*, 5559-5563.

(13) Tang, C.; Tracz, A.; Kruk, M.; Zang, R.; Smilgies, D.-M.; Matyjaszewski, K.; Kowalewski, T. *J. Am. Chem. Soc.* **2005**, *127*, 6918-6919.

(14) Yen, M.-Y.; Chiu, C.-W.;C.; Hsia, C.-H.; Chen, F.-R.; Kai, J.-J.; Lee, C.-Y.; Chiu, H.-T. *Adv. Mater.* **2003,** *15*, 235-237.

(15) Hsia, C.-H.; Yen, M.-Y.; Lin, C.-C.; Chiu, H.-T.; Lee, C.-Y. *J. Am. Chem. Soc.* **2003,** *125*, 9940-9941.

(16) Huang, C.-H.; Chang, Y.-H.; Lee, C.-Y.; Chiu, H.-T. *Langmuir* **2006**, *22*, 10-12.

(17) Brian, J.; Charles, F. K. *J. Sed. Petrol.* **1993**, *63*, 1018-1031.

(18) Guillaume, C.; Olivier, B.; Christophe, D.; Michel, A.; Eric, P. V. *Catena* **2005**, *59*, 1-17.

(19) Leibler, L. *Macromolecules* **1980**, *13*, 1602-1617.

(20) Matsen, M. W.; Bates, F. S. *Macromolecules* **1996**, *29*, 7641-7644.

(21) Bates, F. S.; Fredrickson, G. H. *Annu Rev. Phys. Chem.* **1990**, *41*, 525-557.

(22) Bockstaller, M. R.; Mickiewicz, R. A.; Thomas, E. L. *Adv. Mater.* **2005**, *17*, 1331-1349.

(23) Warren, B. E.; Bodenstein, P. *Acta Cryst.* **1965**, *18*, 282-286.

(24) Vix-Guterl, C.; Couzi, M.; Dentzer, J.; Trinquecoste, M.; Delhaes, P. *J Phys. Chem. B* **2004**, *108*, 19361-19367.

(25) Yoon, S. B.; Chai, G. S.; Kang, S. K.; Yu, J. S.; Gierszal, K. P.; Jaroniec. M. *J. Am. Chem. Soc.* **2005**, *127*, 4188-4189.

(26) Zeng, Z.; Natesan, K. *Chem. Mater.* **2003**, *15*, 872-878.

(27) Dresselhaus, M. S.; Dresselhaus, G.; Pimenta, M. A.; Eklund, P. C. In *Analytical Applications of Raman Spectroscopy*; Pelletier, M. J. Ed.;Blackwell Science: Oxford, **1999**; Chapter 9.

(28) Chieu, T. C.; Dresselhaus, M. S. Endo, M. *Phys. Rev. B* **1982**, *26*, 5867-5877.

(29) Hou, H.; Schaper, A. K.; Jun, Z.; Weller, F.; Greiner, A. *Chem. Mater.* **2003**, *15*, 580-585.

(30) Liu, J.; Shao, M.; Chen, X.; Yu, W.; Liu, X.; Qian, Y. *J. Am. Chem. Soc.* **2003**, *125*, 8088-8089.

(31) Liang, C.; Dai, S.; Guiochon, G. *Anal. Chem.* **2003**, *75*, 4904-4912.

(32) Yan, X.; Liu, G.; Li, Z. *J Am. Chem. Soc.* **2004**, *126*, 10059-10066.

(33) Bockstaller, M. R.; Mickiewicz, R. A.; Thomas, E. L. *Adv. Mater.* **2005**, *17*, 1331-1349.

(34) Colligan, G.; Galasso, F. *Nature* **1961**, *190*, 621-621.

(35) NIST Chemistry WebBook, *http://webbook.nist.gov/chemistry.*

(36) Spino, C.; Pesant, M.; Dory, Y. *Angew. Chem.* **1998**, 37, 3262-3265.

(37) Dewar, M. J. S.; Pierini, A. B. *J. Am. Chem. Soc.* **1984**, *106*, 203-208.

(38) Peter, K.; Vollhardt, C.; Schore, N. E. *Organic Chemistry*, 3rd Edition: Freeman Press, New York, **1998**, p600-p604.

(39) Huang, C.-H.; Lee, C.-Y.; Chang, Y.-H.; Lin, H.-K.; Chiu, H.-T. See in chapter 5.

(40) Kerr, J. A. *Chem. Rev.* **1966**, *66*, 465-500.